

Current Biology

Heuristic Rules Underlying Dragonfly Prey Selection and Interception

Highlights

- Dragonflies use heuristic selection rules to determine which prey to pursue
- Prey angular size and speed, foveation error, and zenith crossing are evaluated
- These rules initialize takeoff for optimal interception flight conditions
- Prey that do not satisfy the rules are usually ignored or pursued unsuccessfully

Authors

Huai-Ti Lin, Anthony Leonardo

Correspondence

leonardoa@janelia.hhmi.org

In Brief

Dragonflies catch rapidly maneuvering prey. The study by Lin and Leonardo shows that dragonflies use heuristic rules to select prey for pursuit. Rules constrain the prey motion statistics and its position relative to dragonfly's gaze and body orientation. This initializes takeoff to the conditions required for a successful interception flight.



Heuristic Rules Underlying Dragonfly Prey Selection and Interception

Huai-Ti Lin¹ and Anthony Leonardo^{1,2,*}

¹Janelia Research Campus, Howard Hughes Medical Institute, 19700 Helix Drive, Ashburn, VA 20147, USA

²Lead Contact

*Correspondence: leonardoa@janelia.hhmi.org

<http://dx.doi.org/10.1016/j.cub.2017.03.010>

SUMMARY

Animals use rules to initiate behaviors. Such rules are often described as triggers that determine when behavior begins. However, although less explored, these selection rules are also an opportunity to establish sensorimotor constraints that influence how the behavior ends. These constraints may be particularly significant in influencing success in prey capture. Here we explore this in dragonfly prey interception. We found that in the moments leading up to takeoff, perched dragonflies employ a series of sensorimotor rules that determine the time of takeoff and increase the probability of successful capture. First, the dragonfly makes a head saccade followed by smooth pursuit movements to orient its direction-of-gaze at potential prey. Second, the dragonfly assesses whether the prey's angular size and speed co-vary within a privileged range. Finally, the dragonfly times the moment of its takeoff to a prediction of when the prey will cross the zenith. Each of these processes serves a purpose. The angular size-speed criteria biases interception flights to catchable prey, while the head movements and the predictive takeoff ensure flights begin with the prey visually fixated and directly overhead—the key parameters that underlie interception steering. Prey that do not elicit takeoff generally fail at least one of the criterion, and the loss of prey fixation or overhead positioning during flight is strongly correlated with terminated flights. Thus from an abundance of potential targets, the dragonfly selects a stereotyped set of takeoff conditions based on the prey and body states most likely to end in successful capture.

INTRODUCTION

It is well established that sensory rules are often used to launch behaviors: many invertebrates will escape from a looming object when the time-to-contact exceeds a threshold [1, 2]; jumping spiders will strike prey when the prey are overhead [3]; and salamanders will project their tongues when prey cross their visual midline [4]. Each of these behaviors, and many others, is triggered at the appearance of an appropriate sensory stimulus

[5, 6]. The onset of behavior can also rely on preparatory movements that orient the body and constrain the sensory and motor state of the animal [7, 8]. The role of such preparatory movements and their integration with sensory selection rules remains unexplored for many behaviors, including prey capture.

The success of a predator should hinge on not just its pursuit strategy but also on the rules it uses to select prey and the time and place it begins pursuit. Prior studies have examined prey capture in terms of energetics [9, 10], behavioral strategies [4, 11–13], biomechanics [14, 15], sensory acquisition [16–18], and ecology [19–22], but the role of initial conditions on prey capture outcome is not well understood. Dragonfly prey capture is one system where selection rules could be used to constrain the initial conditions of each interception flight to increase prey capture success. Dragonflies intercept flying prey using a combination of reactive and predictive control [13]. Steering appears to be based on keeping three variables constant (Figure 1A). First, the dragonfly maneuvers to position prey directly above themselves, at the zenith. Second, the dragonfly rotates its body to match the prey's direction of flight. Finally, the dragonfly rotates its head so it is looking directly at the prey, and holds the prey centered in the high-acuity fovea on its dorsal eye [23]. Once these conditions are established, the dragonfly's steering problem is simplified to matching the prey's speed and steadily moving upward toward the interception point. When the prey deviates from these conditions, the dragonfly maneuvers to re-establish them [13].

The energetic cost of capturing maneuvering prey combined with the complexity of the internal models used for guidance [13] suggest that the initial conditions of the prey's motion and the dragonfly's head and body orientation will influence flight outcome. Consistent with this, it is known that dragonflies make head movements immediately before takeoff [24, 25] (Movie S1) and will pursue prey within only a limited range of distances [23, 26]. However, the purpose of these head movements remains unclear, in part due to the difficulty in using traditional cameras to measure head kinematics relative to moving prey [23–26]. Similarly, it is unknown what pre-takeoff parameters, if any, are predictive of whether a dragonfly will pursue prey and, once in-flight, whether it is likely to succeed in capturing it.

Here we have determined the computations and preparatory movements employed by dragonflies to launch prey interception flights. We used an automated artificial prey presentation system to challenge dragonflies with prey of varying properties, and we used video and motion capture to measure the head and body movements of each dragonfly during both the pre-takeoff period and the interception flight. These data reveal that dragonflies

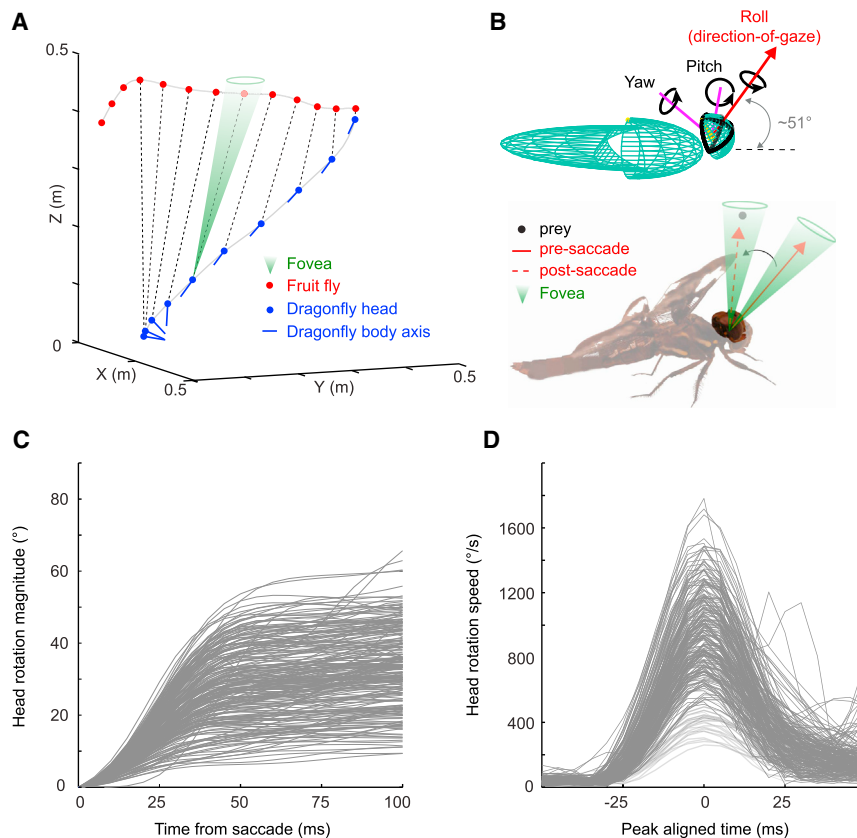


Figure 1. Dragonfly Prey Interception and Pre-takeoff Head Saccades

(A) Example flight path of a dragonfly intercepting a fruit fly. The dragonfly intercepts flying prey by aligning its body and flight path with the prey's direction of motion while positioning itself directly under the prey. During the interception flight, the prey image is held within the high-acuity fovea on the eye.

(B) Most interception flights are preceded by a head saccade. Top: The rotations of the head are described in terms of their Euler angles, with the direction-of-gaze represented by the roll axis, and prey azimuth and elevation relative to the direction-of-gaze represented by the yaw and pitch axes, respectively. At rest, the dragonfly's direction-of-gaze is held at an elevation of $\sim 51^\circ$ from the horizon and is aligned to the body in azimuth. Bottom: Prey passing overhead elicit a head movement that orients the direction-of-gaze toward the prey (post-saccade vector).

(C) Dragonfly head rotation magnitude as a function of time relative to saccade onset ($n = 250$). Head saccades lasted 54 ± 11 ms and had a magnitude of $27.4^\circ \pm 11.8^\circ$.

(D) Dragonfly head saccade speed as a function of time relative to peak speed ($n = 250$). The average rotational speed of the head was of $883^\circ/\text{s} \pm 422^\circ/\text{s}$ (range: $200^\circ/\text{s}$ – $1,700^\circ/\text{s}$).

Further details may be found in [Figures S1, S2, and S3](#). See also [Movies S1, S2, and S3](#).

actively select the position, speed, and size of prey relative to both their head and body, well before takeoff. Errors in this process are correlated with the failure to pursue prey and the termination of on-going flights. Thus dragonflies use a heuristic selection process to create a set of stereotyped sensorimotor takeoff conditions for each flight and then maintain these conditions in-flight to increase the likelihood of successful prey capture.

RESULTS

Dragonflies (*Plathemis lydia*) were released in a large indoor flight arena and presented with either real or artificial prey ([Figure S1A](#)). The artificial prey provided the experimental control needed to map the space of prey movements that would elicit takeoff, while real prey were used to confirm the validity of key results under naturalistic conditions. Real prey (*Drosophila virilis*) were tracked at 1,000 fps with high-speed video; artificial prey (a computer-controlled retroreflective bead) were tracked with motion capture at 200 fps ([Figures S1B–S1D](#)). Dragonfly head movements were detected by high-speed video and, when required by particular experiments, motion capture was used to measure what the dragonfly saw during a prey presentation and the precise three-dimensional (3D) kinematics of the head movements [13]. In these latter cases, small 750- μm retroreflective markers were attached to the dragonfly's head and body and their positions tracked with an array of 18 strobed IR cameras at 200 fps (see [Experimental Procedures](#), [Figures S1A, S1C, S2A, and S2B](#)).

We classified prey presentations into three categories. No-takeoff trials were prey presentations that did not elicit flight from the dragonfly. Successful flights for real prey are those in which the dragonfly physically contacted the prey, and for artificial prey are those in which the dragonfly came within 30 mm of the prey (at less than this distance, the dragonfly pitches its body at least 90° to initiate capture and its tracking markers often become invisible to our cameras; [Movie S2](#)). Terminated flights were defined as all flights that were not successful and were halted well before the point of interception ([Movie S3](#)). 92% of terminated flights ended before the dragonfly was within 100 mm of the prey.

Throughout the paper, all measurements are reported as mean \pm standard deviation (STD), unless otherwise noted.

Head Saccades and Prey Foveation Dynamics

We began by measuring the kinematics of the pre-takeoff head movements in 14 dragonflies over 250 presentations of 2-mm artificial prey that traveled at constant speed with motion statistics comparable to real prey. For a typical prey presentation at 1 m/s, 400 mm from the dragonfly, the prey's angular size and speed were roughly 0.28° and $140^\circ/\text{s}$. While the dragonfly did not move its head to every prey presentation, nearly all takeoffs (95%, 100 of 105 trials) were preceded by a head movement, suggesting they comprise an integral component of the prey selection process. The yaw and pitch of these head movements were controlled independently; yaw and roll had a strong linear correlation (slope 0.66; $r^2 = 0.46$; [Figures S2C and S2D](#)). The

maximum head pitch we observed across 250 trials was 52.3° , the maximum yaw was 76.2° , and the maximum roll was 70.8° . Head movements lasted 54 ± 11 ms, had a speed of $882.9^\circ/\text{s} \pm 421.6^\circ/\text{s}$, and rotated the direction-of-gaze $27.4^\circ \pm 11.8^\circ$ (Figures 1C and 1D). Together, these properties indicate the head motion is stereotyped in time but variable in amplitude and primarily sets a specific azimuth and elevation of the head relative to the body. This is reminiscent of vertebrate eye saccades [27], and we refer to these brief and rapid head rotations before flight as pre-takeoff head saccades.

Prior work has proposed that the dragonfly uses motion parallax from the head movement to estimate the distance to the prey [26]. Other studies have suggested takeoff can occur in the absence of head movements [28]. Parallax requires a translation of the target image across the eye; the magnitude and rate of this movement are monotonic nonlinear functions of prey distance (see Experimental Procedures, Figure S3). Because dragonfly head saccades are primarily rotations, they yield a negligible translation of the head (<0.5 mm). However, the optical center of the eye is offset from the center-of-rotation of the head [26]. This offset causes pure rotations of the head to produce translations of the prey image. The magnitude of these translations is unknown, but it has been suggested the dragonfly might use them to compute prey distance via parallax [26]. To assess this, we estimated the translation of the optical center for each saccade ($n = 165$) and then calculated the resultant parallax angular velocity of the prey image. These image speeds were exceedingly small. In order to discriminate prey at 350 mm from prey at 600 mm (typical versus distant prey) the dragonfly would have to detect a $\sim 10^\circ/\text{s}$ difference in the parallax rate from the ongoing head movement of $\sim 1,000^\circ/\text{s}$ (Figure 1D versus S3B). Moreover, in contrast with the stereotyped head movements used to drive parallax in other insects like locusts and mantids [29, 30], the amplitude of each dragonfly head movement was unique (Figure 1C), further complicating the parallax calculation (see Supplemental Experimental Procedures). Thus while parallax is theoretically possible, these data suggest that the head movements serve an entirely different purpose.

A different hypothesis for role of the pre-takeoff head saccade is that it allows the dragonfly to orient its direction-of-gaze at the prey [24]. During interception flights, dragonflies hold the prey image on a specific region of the head which closely matches the high-acuity fovea on the dorsal portion of the eye [13, 23, 31]. We refer to the ± 1 STD boundaries of this region of image stabilization as the *fovea* (an $8^\circ \times 16^\circ$ ellipse, with the long axis oriented in elevation; Figure 2A, see Experimental Procedures and [13]), the axis normal to the fovea's center as the *direction-of-gaze* (Figure 1B), and the angle between the prey image location and the direction-of-gaze as the *foveation error*. We compared the location of the prey image and the direction-of-gaze immediately before and after the head saccade (Figures 2B–2D). The head saccade moved the dragonfly's direction-of-gaze toward the position of the prey in both azimuth and elevation (Figure 2C, $n = 250$). This initial rotation typically placed the prey image within the fovea but not at its center. The saccade pitch undershot the prey's elevation (slope 0.58, $r^2 = 0.76$; Figure 2C), leaving the prey image either slightly above or below the direction-of-gaze. In contrast, the saccade yaw matched

the azimuth of the prey more closely (slope 0.85, $r^2 = 0.92$; Figure 2C). Undershoots occurred regardless of whether the prey was converging or diverging from the dragonfly's direction-of-gaze, suggesting it is a general property of the saccade controller similar to that seen in other systems [32–34].

Immediately after foveation was established by the saccade, the dragonfly continued to rotate its head to continuously track the moving prey. We examined this process in 9 dragonflies and 165 artificial prey trajectories (see Experimental Procedures). This smooth pursuit tracking generally held prey within the fovea and progressively reduced the foveation error (Figures 2B, 2D, and 2E). However, the direction of smooth pursuit tracking had a characteristic trend: because the initial saccade nearly always undershot the prey's location (Figure 2C), the smooth pursuit continued in the same direction as the saccade, albeit at a considerably slower speed (the angular speed of the prey). Smooth pursuit head tracking lasted 307 ± 119 ms (range 70–885 ms) for trials that led to interception flights (both successful, $n = 39$, and terminated, $n = 65$). For no-takeoff trials, tracking lasted longer: 366 ± 236 ms (range 90–1,425 ms; $n = 61$). In these latter cases the head was returned to its resting position when tracking ended. Smooth pursuit tracking was thus easily distinguished from saccades based on both its speed ($\sim 100^\circ/\text{s}$ versus $\sim 1,000^\circ/\text{s}$) and duration (~ 300 ms versus 50 ms), and it considerably improved the foveation error remaining after the saccade. The foveation error of no-takeoff trials was comparable to that of trials that led to terminated flights. However, trials that led to successful interception had lower foveation error than terminated or no-takeoff trials (Figures 2E and 2F). For example, the average foveation error at takeoff was $3.8^\circ \pm 2.7^\circ$ for successful flights versus $8.8^\circ \pm 9.9^\circ$ for terminated ones. These differences were immediately apparent after the saccade, well before takeoff (one-way ANOVA, $p < 0.05$, Figure 2E), and persisted during the flight (two-sample t test, $p < 0.05$, Figure 2F).

The primary purpose of the head saccade thus appears to be not a parallax measurement [23, 26] but rather a series of gestures to center the prey image on the fovea of the dragonfly's visual system [24], the location where it will be held throughout the interception flight itself [13]. Consistent with this, when we examined the roughly 5% of interception flights that occurred in the absence of a pre-takeoff head movement, we found that prey were still foveated at the moment of takeoff. In these cases the prey trajectory intersected with the fovea in the head's resting position, and no saccade was needed.

Takeoff Is Timed Predictively to the Prey Crossing above the Dragonfly

The dragonfly selected prey whose flight paths evolved systematically during the 300 ms between the head saccade and takeoff. We pooled data across prey presentations ($n = 165$) so we could identify the volume of space where prey were typically located, relative to the dragonfly's body (rather than the moving reference frame of the head, Figure 2), at different moments before and after takeoff. We found that at each moment in time before takeoff, prey were not distributed randomly in space but were instead located above the perched dragonfly in a conical volume (Figure 3). The centroid axis of this volume is a vector directed upward and forward relative to dragonfly's body. We

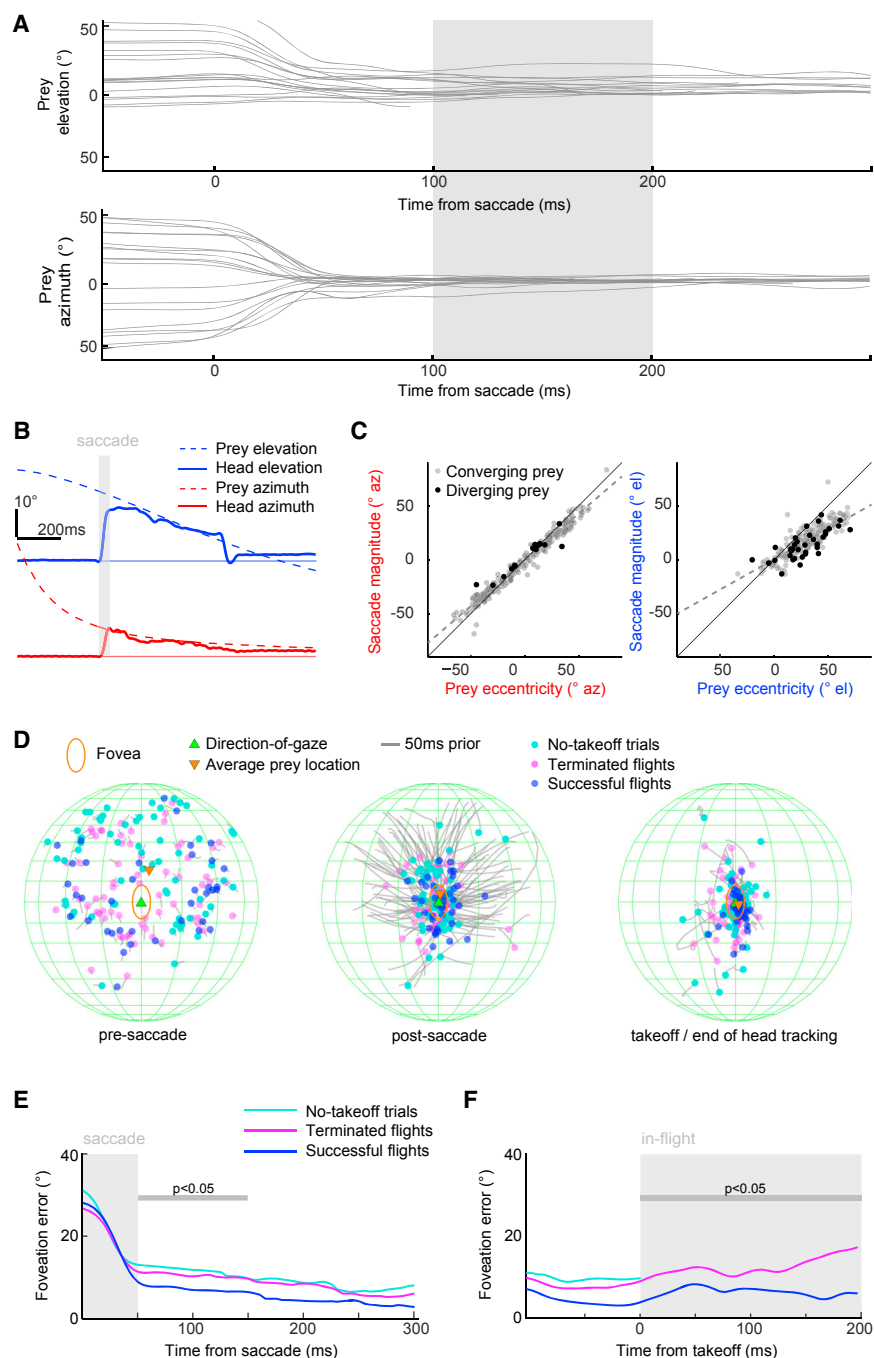


Figure 2. Head Saccade and Smooth Pursuit Tracking Foveate the Prey before Takeoff

(A) Time series of prey position in the head reference frame (see Figure 1B) for one dragonfly, relative to saccade onset, across 19 trials. The gray box defines the time interval in which the fovea (± 1 -std boundaries) and direction-of-gaze (mean positions) were defined for this animal.

(B) Prey position and dragonfly head orientation in the lab reference frame, in elevation and azimuth, for one trial. A rapid head saccade orients the direction-of-gaze toward the prey. The head saccade is followed by a period of smooth pursuit tracking that holds the prey's position close to the direction-of-gaze. At the cessation of smooth pursuit tracking, the head returns to roughly its resting position.

(C) Scatterplot of head saccade magnitude in azimuth (left) and elevation (right) as a function of prey eccentricity (on the head) at saccade onset ($n = 250$). There is more undershoot in elevation than azimuth, regardless of whether prey are converging toward or diverging from the direction-of-gaze.

(D) Spherical plots of prey position relative to the dragonfly's direction-of-gaze, as a function of time and trial outcome for 165 trials and 9 dragonflies. All data points show the 50 ms of prey image motion leading up to the time shown, plotted as gray lines.

(E and F) Time series of average foveation error relative to saccade onset (E) and takeoff (F) for trials with no-takeoff ($n = 61$), terminated flights ($n = 65$), and successful interception flights ($n = 39$). Foveation error after the head saccade was 9° for trials that led to successful interception, versus 14° (terminated flights) or 12° (no-takeoff). At takeoff, successful flights had a foveation error of 4° , versus 9° for terminated flights. Grey bars show time windows over which statistical tests were performed. Shortly after the saccade, foveation errors were significantly different for no-takeoff trials, terminated flights, and successful flights (one-way ANOVA, $p < 0.05$). After takeoff, the foveation error for successful flights were significantly smaller than those for terminated flights (two-sample t test, $p < 0.05$).

See also Figures S1, S2, and S3 and Movie S1.

characterized the prey cone by its *orientation* (the angular offset of the centroid axis from the zenith in elevation), its *overhead error* (average angle between prey and the centroid axis), and its *boundaries* (± 2 STD, in azimuth and elevation, from the centroid axis).

We focused first on the evolution of the prey cone during successful interception flights (Figures 3A and 3C; $n = 39$). At the onset of the head saccade, prey were distributed in a cone with boundaries of $112^\circ \times 88^\circ$ (azimuth \times elevation) and tilted 15° forward from the zenith (Figure 3A). The head saccade was triggered by prey movement in any direction within this region, which we

refer to as the saccade cone. As smooth pursuit head tracking progressed and the moment of takeoff approached, prey flew inward toward the space directly above the dragonfly. Consequently the prey cone shrank and its axis rotated toward the zenith. At takeoff, prey were found in a cone with boundaries of $57^\circ \times 45^\circ$ ($\sim 50\%$ width of the saccade cone), with its axis tilted only 10° forward from the zenith (Figure 3C); we refer to this as the takeoff cone. Real prey ($n = 142$) that were successfully captured were found within a takeoff cone similar to that of artificial prey (Figure 3C). As the time from saccade to takeoff progressed, the expected prey position thus converged toward the

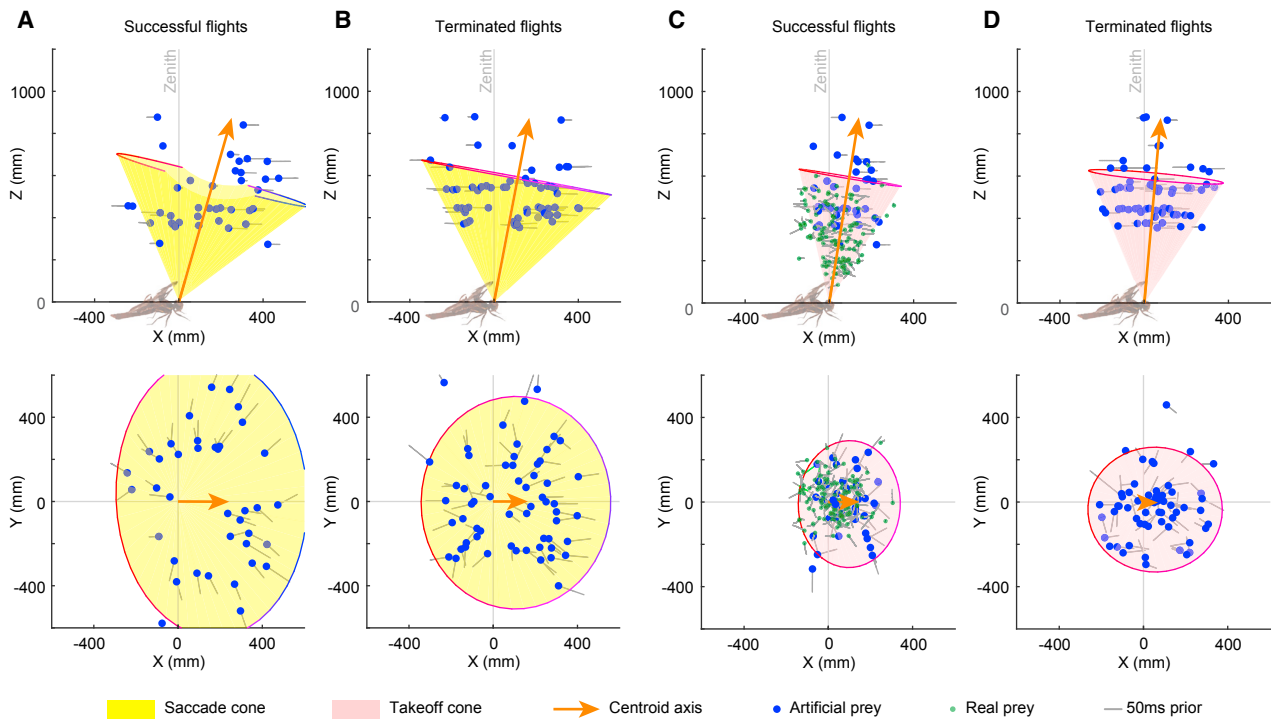


Figure 3. Prey Are Positioned Directly above Dragonfly as Takeoff Approaches

Scatterplots of prey position relative to dragonfly's perched body position in global coordinates (with the dragonfly's head at the origin and its body orientation aligned to the x axis; 104 trials, 9 dragonflies). Shaded regions indicate ± 2 STD boundaries of a cone fit to the data, and lollipops show individual prey locations with direction of motion toward the dot. These volumes correspond to the stationary body reference frame, versus those in Figure 2 which correspond to the moving head reference frame.

(A) Saccade cone, successful flights. For successful flights, saccades occur as prey are moving in a cone of $88^\circ \times 113^\circ$ wide (at the 2 STD) and tilted 15° forward from the zenith (gray line).

(B) For terminated flights, the saccade cone is slightly smaller ($86^\circ \times 88^\circ$) with axis closer to the zenith (10° forward).

(C) Takeoff cone, successful flights. For successful flights at the moment of takeoff, prey are tightly clustered above the dragonfly ($45^\circ \times 57^\circ$ cone boundaries oriented 10° forward of zenith). Real prey cluster in the same cone as fit to artificial prey.

(D) For terminated flights, the takeoff cone is $59^\circ \times 48^\circ$ oriented 7° forward from the zenith.

See also Figure S1.

zenith with increasing accuracy and precision (Figures 4A and 4B). However, the minimum overhead error was not reached at takeoff, but 65 ms after takeoff (overhead error, 15° ; orientation, 6° forward of zenith; Figures 4A and 4B). Examination of video records showed that at this time, during successful flights, the dragonfly was just fully in-flight, roughly 1 cm off the ground and directly below the prey (Figure 4C).

In contrast to successful flights ($n = 39$), terminated flights ($n = 65$) showed a different evolution of the prey cone from saccade to takeoff (Figures 3B and 3D). In these cases, the prey cone orientation approached the zenith considerably earlier and shifted substantially away from the zenith after the dragonfly was in flight (t test, $p < 0.05$, Figure 4A). Terminated flights reached a minimum overhead error 10 ms before takeoff (Figure 4B) rather than 65 ms after takeoff as seen for successful flights. In short, when the dragonfly took flight, prey were directly overhead during successful flights and were dispersed and diverging outward during terminated flights (Figures 3C, 3D, 4A, and 4B; Movies S2 and S3). This characteristic evolution in the size and orientation of the prey cone, from saccade to takeoff, did not arise from any action by the dragonfly but instead

from its selection of prey whose flight paths steadily converged inward toward the overhead position.

The precision and accuracy of prey localization, relative to the dragonfly's zenith, was maximized after takeoff. However, sensory transduction to detect prey position and the motor action to engage the wings take considerable time. This suggests that the dragonfly must prepare for the overhead crossing well in advance and time its takeoff accordingly. If the dragonfly did not anticipate the overhead crossing but instead reacted to prey that reached the overhead position, the prey would be dispersed by the time dragonfly was in-flight. To evaluate this, we examined the timing of the leg and wing gestures that drove the takeoff. We defined the moment of takeoff ($t = 0$) as the vertical acceleration peak in the first downstroke of the wings (Figure 4C). The acceleration of the dragonfly's body began rising 50 ± 17 ms before takeoff, indicating it had already committed to a flight by initiating leg movements and the wing upstroke. The response latency of visual neurons thought to register the approach of the prey is roughly 25 ms [35]. We conclude from this that the dragonfly's actions predict the moment of overhead crossing at least 140 ms into the future: 75 ms pre-takeoff

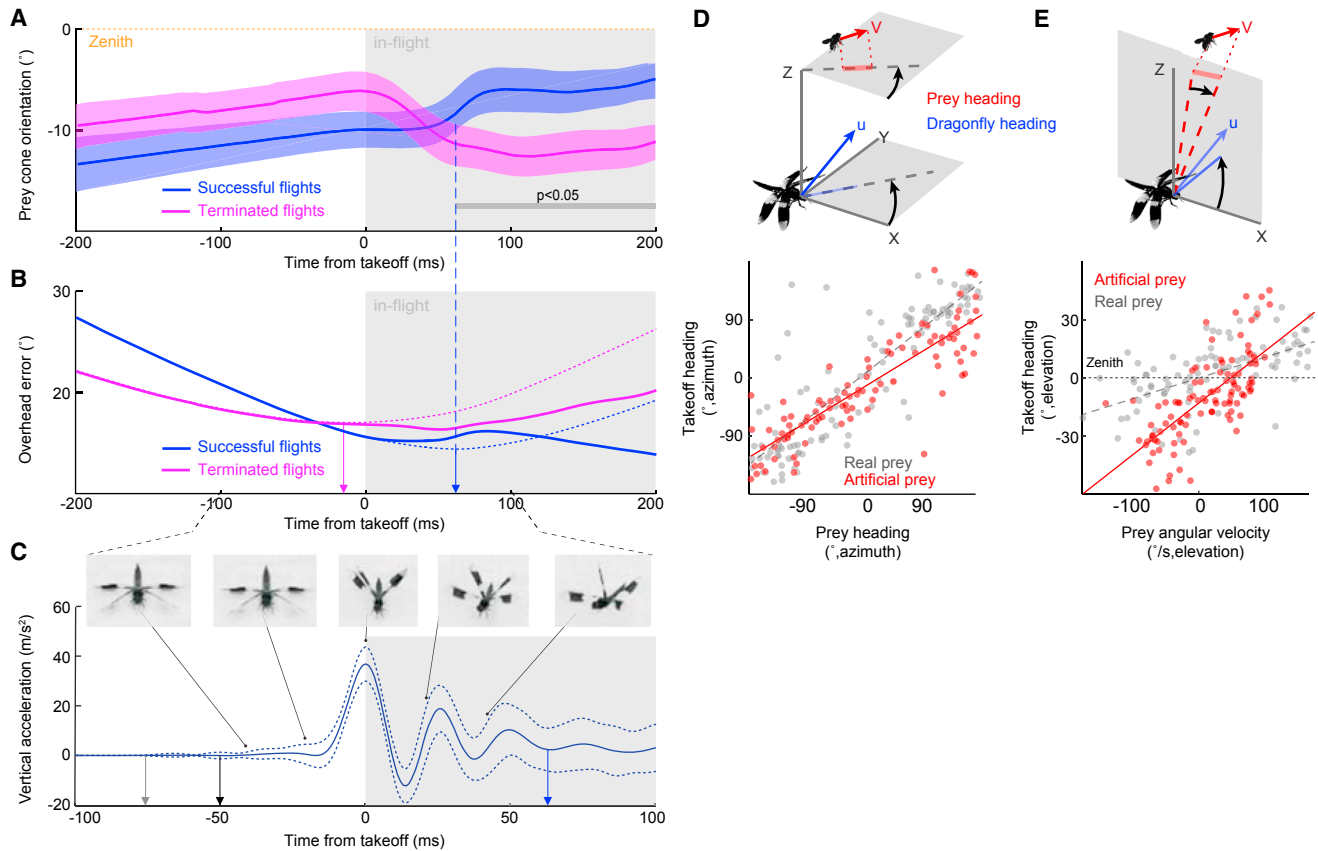


Figure 4. Takeoff Timing Anticipates Approach of Prey to Zenith

(A) Prey cone orientation relative to takeoff for successful ($n = 39$) and terminated ($n = 65$) flights. Prey are typically farther from the zenith for successful versus terminated flights prior to takeoff (mean \pm SEM). However, after takeoff, prey converge toward the zenith for successful flights and diverge away from the zenith for terminated flights (gray bar indicates time window 65 ms after takeoff; two-sample t test, $p < 0.05$).

(B) Prey overhead error, the average offset of prey from the prey cone centroid axis, as a function of time. Solid lines show the overhead error the dragonfly experienced (including the moving reference frame after takeoff); dashed lines show the expected error in the fixed reference frame of the dragonfly's perched location. The expected overhead error was minimized 65 ms after takeoff during successful flights. In contrast, for terminated flights, the expected overhead error reached its minimum 10 ms before takeoff.

(C) Dragonfly vertical acceleration (mean \pm STD, solid and dashed lines, $n = 142$) and kinematics (video frames) relative to takeoff, defined as the first peak in acceleration. At 65 ms post-takeoff, the overhead error minima in (B), the dragonfly is fully in-flight. Pre-takeoff gestures, as shown by non-zero acceleration, begin at least 50 ms before takeoff (black arrow). The visual delay is around 25 ms (gray arrow) [35]. Overall, this suggests that the dragonfly anticipates the prey overhead crossing at least 140 ms into the future (gray arrow to magenta arrow).

(D) Takeoff direction in azimuth is a linear function of prey direction in azimuth, for artificial prey ($r^2 = 0.77$, $n = 104$) and real prey ($r^2 = 0.77$ also, $n = 142$).

(E) Takeoff direction in elevation is linearly correlated to the prey angular velocity in elevation for artificial prey ($r^2 = 0.50$, $n = 104$) and real prey ($r^2 = 0.54$, $n = 142$). See also Figure S1.

response (25 ms visual latency and 50 ms leg/wing movement) and 65 ms post-takeoff wing movement to get into the air roughly timed to the prey's overhead crossing. The complexity of this prediction, and its reliance on prey angular velocity, remain to be determined. Because the takeoff reaction time is ~ 75 ms, this should be the minimum duration for the head saccade and smooth pursuit tracking interval. Consistent with this, the shortest duration from head saccade to takeoff in our dataset was 70 ± 5 ms.

In addition to coordinating the moment of takeoff, the dragonfly launched itself in a direction strongly correlated with the prey's direction of motion. The dragonfly's heading in azimuth was a linear function of the prey's heading in azimuth (Figure 4D). Such a directional takeoff will contain preparatory leg and wing

gestures, reminiscent of those seen in directional escape takeoffs [7]. The dragonfly's heading in elevation was a linear function of the prey's angular velocity (relative to the dragonfly, in elevation; Figure 4E). These heading parameters allowed the dragonfly to rapidly align its body axis to the prey's direction of motion, while maintaining the position of the prey overhead.

Prey Viability Is Assessed via Angular Size and Angular Speed

While the analysis thus far has focused primarily on prey position (Figures 2, 3, and 4), prey distance and speed also influence the probability of interception success (Figure 5A). Longer prey distances and faster prey speeds require longer flight times and higher top speeds to attain capture. Consequently, some prey

will be too far or fast to be captured. We found that perched dragonflies pursued nearby *Drosophila* at distances of 100–700 mm, moving at speeds of 0.3–2 m/s (mean distance 361 ± 130 mm; mean speed 1.1 ± 0.3 m/s; Figures 5B and 5C). These ranges suggest that the dragonfly has a method to estimate prey motion statistics. Previous work has proposed that dragonflies compute prey distance via parallax induced by pre-takeoff head movements [26]. Our analysis shows that these movements are in fact optimized for foveation (Figure 2). This suggests that rather than parallax, a different mechanism lets the dragonfly assess prey distance and speed. We sought to uncover this mechanism by systematically mapping the prey motion statistics that elicited takeoff.

We examined four key prey variables: distance (m), speed (m/s), angular size ($^{\circ}$), and angular speed ($^{\circ}/s$). The first two quantities constrain the time-to-capture and dragonfly's maximum interception speed (Figures 5B and 5C). We refer to them as metric distance and metric speed to distinguish them from their angular counterparts. The second two quantities are angular properties that the dragonfly can measure on its eye and can be used to infer the metric distance and speed or simply to constrain the takeoff conditions heuristically. To discriminate between these options, we manipulated all four variables concurrently. In the first experiment (Figures 5D–5F; ~ 9 dragonflies, see Experimental Procedures), we presented artificial prey spanning a wide and uniformly sampled range of angular sizes and angular speeds (0.18° – 0.7° , $30^{\circ}/s$ – $900^{\circ}/s$), corresponding to a wide range of distances and speeds (170–590 mm, 0.1 m/s–7.3 m/s). While nearly all of the artificial prey elicited a head saccade (Figure 5E), only a limited range evoked a takeoff (214 of 1,400 prey presentations). This confirms that a strong selection process was at work and demonstrates that most prey that are not pursued are detected by the dragonfly but deliberately not selected for interception. In general, prey were selected if their angular size and angular speed had a positive correlation to each other (though highly nonlinear, $r^2 < 0.3$ for linear regression for the data in Figure 5E). Prey with larger angular sizes were selected for pursuit at faster angular speeds, and prey with small angular sizes were selected for pursuit at slower angular speeds (Figure 5E). Co-varying the angular size with angular speed in this manner limited the metric speed and distance of the artificial prey to the range of speeds and distances of real prey that were successfully captured (Figure 5F).

Next we sought to determine whether the dragonfly computed prey distance and speed from its angular size and angular speed. Metric and angular parameters co-vary—increasing prey distance implies decreasing prey angular speed. This coupling means it is difficult to determine which of these parameters are important for prey selection. To address this, we presented the dragonfly with artificial prey that decoupled the metric and angular statistics (Figures 5G–5I; ~ 15 dragonflies, see Experimental Procedures). We kept the angular size and angular speed within the range that elicited takeoffs (Figure 5H) but let the metric distance and speed increase substantially over those found for *Drosophila* (maximum altered distances 1.1 m versus 0.7 m *Drosophila*; maximum altered speed 7 m/s versus 2 m/s *Drosophila*; Figure 5I). The dragonfly would need to fly at extremely high speeds and for long flight times to capture these altered prey. For example, prey moving at 7 m/s would require

the dragonfly to fly at 14 m/s (extrapolated from Figure 5C), significantly faster than we have observed (4 m/s max). Likewise, a distance of 1.1 m would require a capture time longer than 515 ms (extrapolated from Figure 5B), considerably more than the average prey interception time (348 ± 110 ms).

If the dragonfly can determine prey metric speed and distance, it will avoid artificial prey that are too fast or too distant to be captured. In contrast, if it knows only the angular parameters, the dragonfly will still pursue the fast and distant artificial prey. The results of this test were unequivocal: the dragonfly readily pursued the fast and distant prey (Figure 5I)—all that was required was for the prey to have appropriate angular speed given its angular size (Figure 5H). Moreover, none of these artificial prey were caught and the dragonfly always terminated its flight well before the point of interception. Thus, the selection of viable prey appears to be based on the angular properties of prey motion rather than true distance or speed estimation strategies such as parallax [29, 36] or stereopsis [37].

The angular properties underlying the selection of real prey (*Drosophila*) were similar but not identical to those of artificial prey. The range of artificial prey angular sizes and speeds selected for pursuit fully encompassed and was larger than the distribution seen for *Drosophila* (Figure 5E). This suggests that the prey selection process is broadly tuned across potential prey and *Drosophila* occupy a subspace of this larger function. Additionally, when we present artificial prey over a wide range of speeds and distances, we obtain insight into what the dragonfly is capable of capturing. This matches surprisingly well with the distance and speed statistics seen for *Drosophila* (Figures 5I versus 5F). Together these observations suggest that the dragonfly uses a model of prey angular properties that is broadly tuned across the prey motion statistics that are found at the speed and distance ranges the dragonfly is capable of intercepting successfully.

Prey Foveation, Overhead Position, and Motion Statistics Predict Most Flight Outcomes

Good prey selection should increase the likelihood of successful capture by eliminating the pursuit of prey likely to be missed. We have identified four parameters that appear to be relevant for selecting prey: foveation error represents the absolute offset of the prey-image from the direction of gaze (Figure 2); overhead convergence represents the rate at which the prey approach the centroid axis of the prey cone (with negative numbers indicating convergence and thereby predicting zenith crossing; Figure 4); prey angular size and angular speed indicate the approximate metric distance and speed of the prey prior to takeoff (Figure 5E). If these parameters are important, then failure to apply them correctly should have behavioral consequences. In prey presentations where these parameters fall below a critical threshold, the dragonfly should not take off and should instead wait for a more suitable target. Alternatively, if the dragonfly pursues prey that do not satisfy the takeoff parameters, there should be a higher rate of terminated flights compared to flights that do satisfy them. We examined both of these possibilities.

We used a bootstrap analysis ($n = 50$, see Experimental Procedures) to select the 100 ms time window (50 – 150 ± 10 ms post-saccade) and thresholds for foveation error, overhead

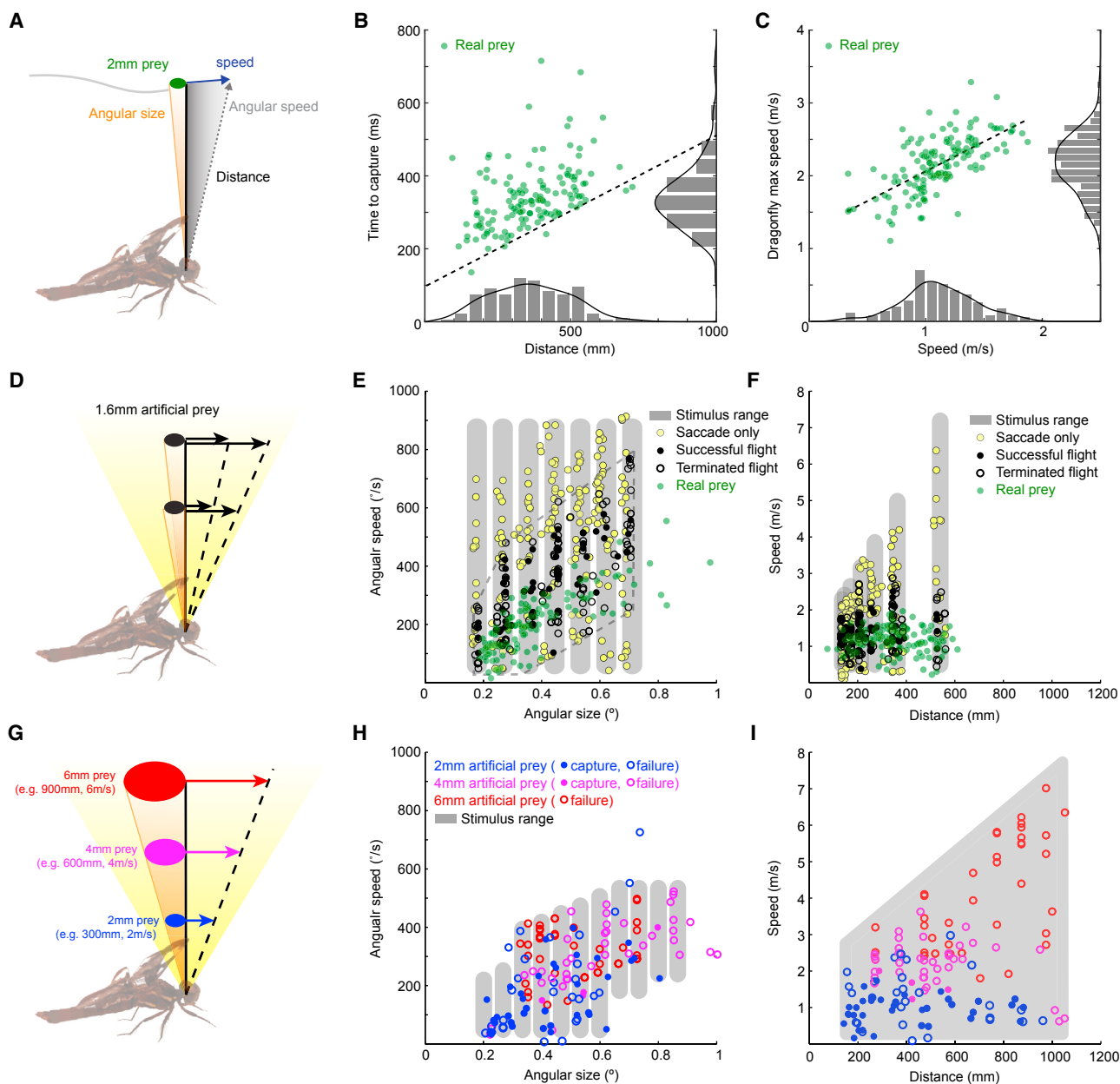


Figure 5. Prey Selection Is Based on Prey Angular Size and Angular Speed

(A) Prey flight statistics are measured when they are directly above the dragonfly, as would occur during takeoff.

(B) Increased prey distance increases the time to capture (142 trials, 18 dragonflies foraging on fruit flies). The marginal distributions of each parameter are shown on their respective axes. The average prey distance at takeoff is 361 ± 130 mm and the average time to capture is 348 ± 110 ms. Dashed line: The 2-STD lower bound for time-to-capture as a function of distance is fit to a straight line.

(C) The maximum flight speed of the dragonfly is a linear function of average prey speed (slope 0.81; intercept 1.3 m/s; $r^2 = 0.43$; data as in B). The marginal distributions of each parameter are shown on their respective axes. The mean prey speed is 1.1 ± 0.3 m/s and the mean dragonfly speed is 2.2 ± 0.4 m/s.

(D) 1.6 mm artificial prey spanning a uniformly sampled range of angular sizes and angular speeds are presented to the dragonfly (≥ 9 dragonflies, see [Experimental Procedures](#)) while head saccades and takeoffs are measured.

(E) Scatterplot of dragonfly responses as a function of the angular prey parameters shown in (D). Grey bars show the stimulus presentation range sampled by the artificial prey (see [Experimental Procedures](#)). Dots show dragonfly head saccades ($n = 557$), terminated flights ($n = 135$) and successful flights ($n = 79$) to artificial prey, and successful flights to real prey ($n = 142$). Dashed region indicates the limited range of prey the dragonfly selects for pursuit.

(F) Scatterplot of dragonfly responses as a function of metric prey parameters for the data shown in (E). Artificial prey are pursued only in a restricted range of speeds, similar to that seen for real prey. Grey bars show the stimulus presentation range of the artificial prey.

(G) Prey angular size and angular speed are held fixed within the selection region shown in (E). Metric prey size, speed, and distance are varied, thereby creating prey with normal angular parameters but uncatchable metric parameters (>15 dragonflies, see [Experimental Procedures](#)).

(legend continued on next page)

convergence, and prey angular size that best discriminated takeoffs for successful captures ($n = 39$) from no-takeoff prey presentations ($n = 61$). We limited the range of prey angular speeds in this experiment ($50^\circ/\text{s}$ – $300^\circ/\text{s}$) to the selection range demonstrated earlier (Figure 5E) to reduce the permutation space of the other three parameters. We found that individual parameters had low discriminatory power (Figures 6A, 6B, and 6E), $89\% \pm 5\%$ of takeoffs had a foveation error $<14^\circ \pm 1.5^\circ$; however, this threshold had a false positive rate of $67\% \pm 7\%$ for no-takeoff trials. Similarly, $92\% \pm 4\%$ of takeoffs had an overhead convergence rate $<-40^\circ/\text{s} \pm 8^\circ/\text{s}$ but had a false positive rate of $55\% \pm 7\%$ for no-takeoff trials. Angular size was larger than 0.13° for $95\% \pm 4\%$ of takeoffs but had a false positive rate of $58\% \pm 6\%$. Combining these parameters into doublets substantially decreased the false positive rate while only mildly affecting the true positive rate. When all three parameters were used together, $76\% \pm 7\%$ of takeoffs were selected correctly and only $28\% \pm 7\%$ of no-takeoff flights had foveation, prey convergence, and angular size values that were consistent with those that led to successful flights (Figure 6E).

We performed a similar analysis to quantify to what extent each selection feature was predictive of a successful ($n = 39$) or terminated ($n = 65$) flight after takeoff. Once again we used three parameters. Foveation error was used as described above. Since prey were generally already directly overhead at takeoff, we examined the overhead error (as in Figure 4) rather than the overhead convergence. Once in flight, prey angular size begins to increase systematically. The angular expansion rate indicates the impending contact with the prey. Using the bootstrap method described above, we sought a time window and a set of thresholds for each of these parameters that could predict whether flights would succeed. Since most terminated flights ended in the 200 ms after takeoff (56 of 61 trials), we found that a 100 ms window shortly after takeoff (125 – 225 ± 12 ms) provided the best discriminatory power across trials. As with the takeoff analysis, individual parameters had both high true positive and false positive rates (Figures 6C, 6D, and 6F). $97\% \pm 3\%$ of successful flights had foveation error of less than $15^\circ \pm 0.5^\circ$, but so did $65\% \pm 7\%$ of terminated flights. $94\% \pm 4\%$ of successful flights had an overhead error of less than $23^\circ \pm 1^\circ$, but with a false positive rate of $75\% \pm 9\%$ for unsuccessful flights. $98\% \pm 2\%$ of successful flights had an angular expansion of more than $0.2^\circ/\text{s} \pm 0.005^\circ/\text{s}$, but with a false positive rate of $75\% \pm 9\%$ for unsuccessful flights. Combining these parameters into doublets progressively reduced false positive rates while only slightly affecting true positives (Figure 6F). When all three parameters were used together, $81\% \pm 6\%$ of successful flights were selected correctly, and only $18\% \pm 5\%$ of terminated flights had foveation error, overhead error, and angular size expansion values that were consistent with those that led to successful flights (Figure 6F). Thus while individual parameters typically satisfy the thresholds on most flights, during

terminated flights at least one of three parameters was outside the range seen for successful flights.

DISCUSSION

A perched dragonfly is confronted by a wide range of possible targets, moving in different directions and at different distances, speeds, and sizes. Only a small number of these targets will be prey that can be caught, and selection is therefore critical. However, the time available to assess prey viability is brief, and the dragonfly uses this period to implement a sophisticated prey selection strategy (Figure 7). Prey moving at $150^\circ/\text{s}$ (i.e., 400 mm range, 1 m/s) will travel from the periphery of the saccade cone to the zenith in roughly 300 ms. We have found that the dragonfly uses this 300 ms period carefully, filling it with a series of preparatory motor gestures, predictions, and estimates that allow it to select prey for pursuit that are likely to be captured and to disregard prey that are likely to be missed (Figure 7). Upon detecting movement in the sky above, the dragonfly makes a 50 ms head saccade to orient its direction-of-gaze at the prey (Figure 2; Movie S1). Prey are then smoothly tracked by the head for another 250 ms, further improving foveation until the prey is held within $\pm 4^\circ$ of the direction-of-gaze (Figures 2D–2F). Simultaneously, the dragonfly assesses the prey's angular size and speed, and if they are in the correct range (Figure 5E), predicts the moment when the prey will pass overhead (Figures 4A and 4B). The takeoff is timed to coincide with this moment (Figures 3C and 4C), and the launch direction is coordinated to the prey velocity vector (Figures 4D and 4E). The prey-image remains foveated and held overhead for the remainder of the interception flight (Figure 2D and [13]). Prey foveation, overhead positioning, angular size, and angular speed are thus actively monitored by the dragonfly, and when their values do not satisfy specific thresholds, the dragonfly either avoids takeoff or terminates the flight well before the interception point (Figures 6E and 6F).

While prey foveation and overhead positioning are improved continuously throughout the 300 ms pre-takeoff period, it is unclear when and how prey angular size and speed are assessed. The dragonfly will make head saccades to a much broader range of prey angular sizes and speeds than that to which it will take off (Figure 5E). This indicates that prey motion statistics are evaluated before foveation but further improved afterward during the smooth pursuit tracking phase. Takeoffs are triggered as quickly as 70 ms post-saccade and as long as 885 ms; the extent to which the accuracy of the angular size and angular speed measurement is refined during this period, or evidence is integrated [38], should be explored in future work. The measurement of prey angular size itself requires fine-scale resolution; prior to takeoff, the prey image always remains below or near the limiting angular resolution of the dragonfly's dorsal fovea: 0.24° – 0.5° [31, 39, 40]. Despite this, prey selection shows a smooth, near linear dependence on prey angular size. Prey of 0.3° , for

(H) Scatterplot of dragonfly responses as a function of the angular prey parameters illustrated in (G). Successful and terminated flights are interspersed. Grey bars show the stimulus presentation range.

(I) Scatterplot of dragonfly responses as a function of the metric prey parameters show in (G). Successful flights occur only for low-speed and -distance prey, comparable to that seen for real prey. However, the entire range of stimuli elicits takeoffs, indicating the dragonfly does not know the underlying metric parameters accurately enough to avoid pursuit of the uncatchable prey. Grey bars show the stimulus presentation range. See also Figure S1.

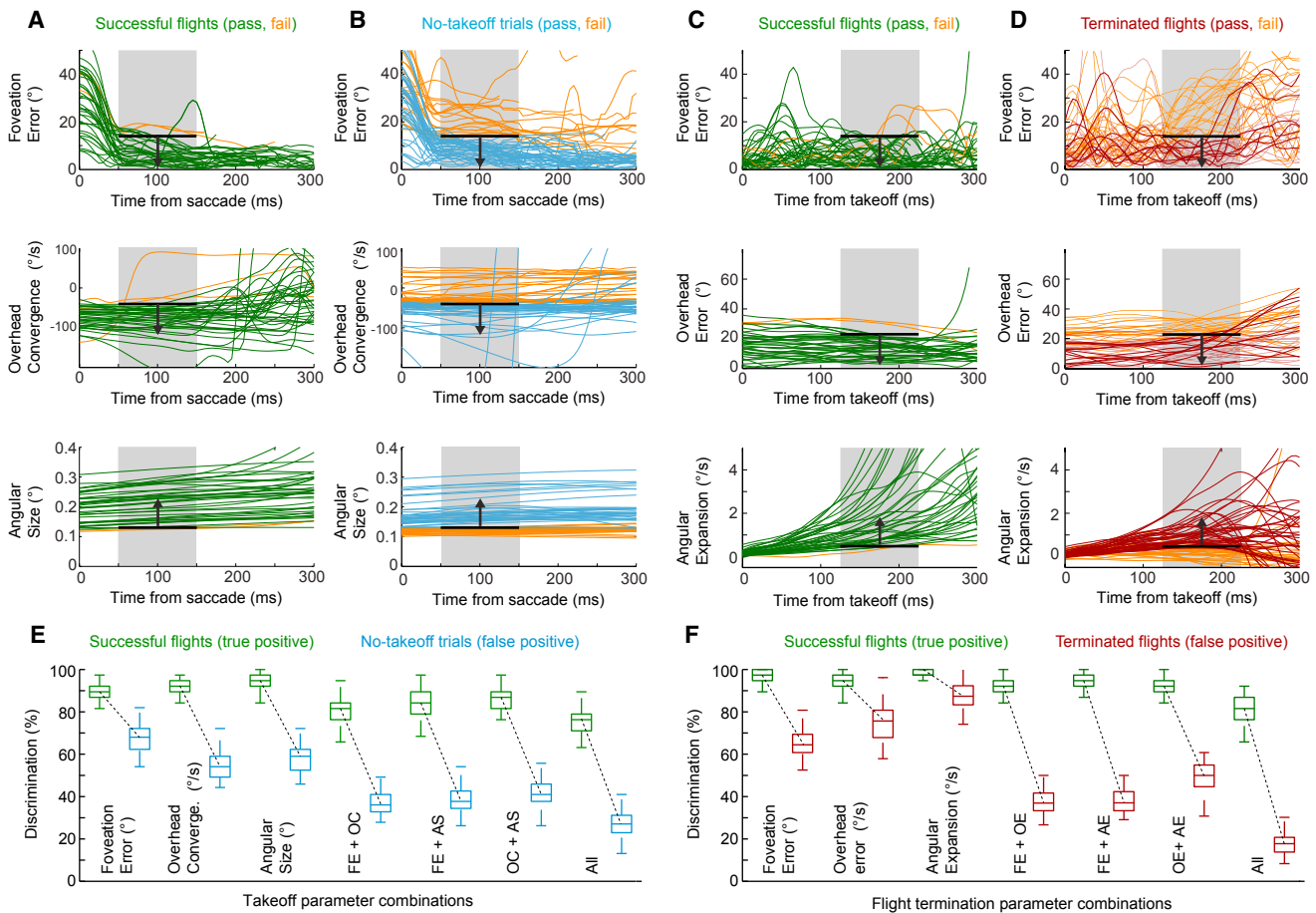


Figure 6. Heuristic Criteria Predict Interception Flight Outcome

Take off and successful interception ($n = 39$) can be discriminated from no-takeoff ($n = 61$) and terminated flights ($n = 65$) based on key parameters.

(A) Time series overlay of foveation error (FE), overhead convergence (OC), and prey angular size (AS) relative to saccade onset for successful flights. Each parameter is color coded per trial based on whether its mean across time in the gray box is above or below a critical threshold (black horizontal line, see [Experimental Procedures](#)).

(B) Time series overlay of foveation error (FE), overhead convergence (OC), and prey angular size (AS) relative to saccade onset for no-takeoff trials. Thresholds are identical to those shown in (A); trials are color coded by whether they are above or below threshold.

(C) Time series overlay of foveation error (FE), overhead error (OE), and prey angular expansion (AE) relative to takeoff for successful flights. Each parameter is color coded per trial based on whether its mean across time in the gray box is above or below a critical threshold (black horizontal line, see [Experimental Procedures](#)).

(D) Time series overlay of foveation error (FE), overhead error (OE), and prey angular expansion (AE) relative to takeoff for terminated flights. Thresholds are identical to those shown in (C), trials are color coded by whether they are above or below threshold.

(E) Discrimination accuracy for successful flight takeoffs (true positives) versus no-takeoffs (false positives) using the thresholds in (A), for all singlet, doublet, and triplet parameter combinations. Each box shows mean \pm STD, as determined by bootstrapping (see [Experimental Procedures](#)). Foveation error, overhead convergence, and prey angular size together provide the best discrimination power.

(F) Accuracy by which successful flights (true positives) are discriminated from terminated flights (false positives) using the thresholds in (C), for all singlet, doublet, and triplet parameter combinations. Each box shows mean \pm STD, as determined by bootstrapping (see [Experimental Procedures](#)). Foveation error, overhead error, and prey angular expansion together provide the best discrimination power.

See also [Figures S1](#) and [S2](#).

example, are pursued at slightly lower angular speeds than prey of 0.5° . Whether this acuity is based on luminance or contrast differences [40], hyperacuity [41, 42], or a different mechanism is unknown. Regardless, prey angular size and angular speed are critical—they place heuristic constraints on prey metric distance and speed [43, 44], rather than explicitly computing them [26, 45]. Although either angular parameter alone is a poor indicator of distance or speed, their combination restricts the selection

to specific motion statistics and they effectively serve as a model of viable prey.

The specialized high-acuity foveal regions on the insect eye are well known [46, 47], but their functional role has rarely been explored during walking and flying behaviors due to the difficulty in reconstructing what the eye sees when it is moving [48]. The miniaturized motion capture system we have developed to solve this problem, used here and in prior studies [13], highlights three

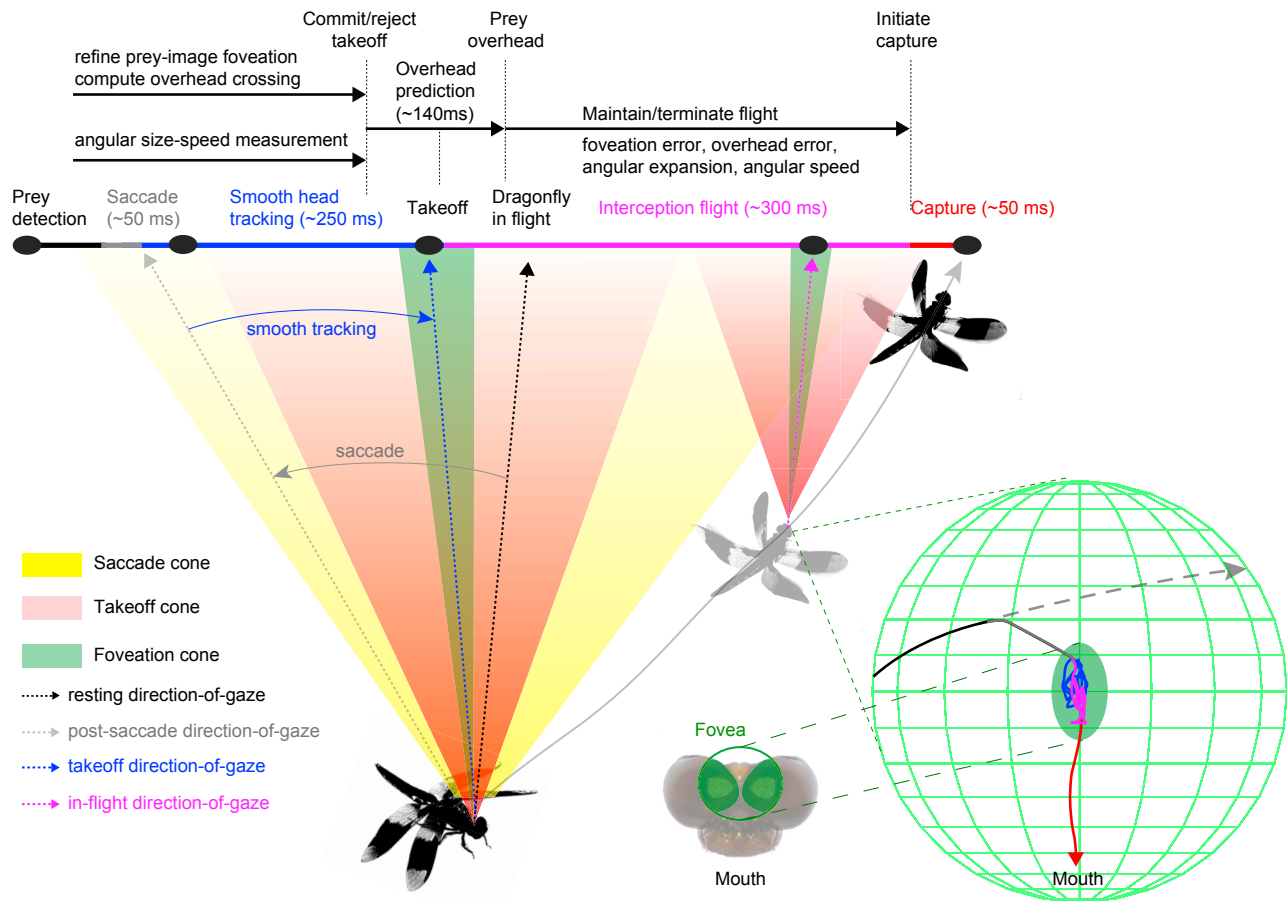


Figure 7. Summary Schematic of Heuristic Rules for Dragonfly Prey Selection and Interception

The dragonfly observes a $\sim 90^\circ$ cone of space for prey. Upon prey detection, a 50 ms head saccade orients the direction-of-gaze toward the prey and places the prey image within the fovea. Smooth pursuit head movements further refine this foveation over the next 250 ms until prey are within $\pm 4^\circ$ of the direction-of-gaze. If foveation error, overhead crossing, and prey angular size and angular speed are acceptable, the dragonfly begins the motor gestures needed to take off. Takeoff is timed to anticipate the prey being directly overhead. After takeoff, the dragonfly maintains foveation by rotating its head predictively to null prey motion and self-motion. The body is steered to hold the prey directly above and align the dragonfly's body axis and flight direction to the prey's flight path. Right inset: prey image trajectory on the head, before and during flight. Top inset: timeline showing different behavioral stages, from prey detection to prey capture, and the approximate onset and duration of each measurement used for prey selection. Flight termination can occur at any time prior to capture. All objects and time bars are drawn for illustration and may not be to scale.

See also [Movies S1](#), [S2](#), and [S3](#).

potential roles the dragonfly fovea plays during prey interception. First, foveation serves an important role in interception guidance [13]. During flight, stabilizing the prey image on the fovea allows the dragonfly to measure unexpected prey movement separately from its own self-motion, facilitating smaller, faster corrections in the flight path. The optical acuity of the fovea is relatively homogeneous and roughly $3\times$ better than the periphery of the eye [31], so the exact position of stabilization is less crucial than that it be somewhere within the fovea. Second, the takeoff decision is based in part on an accurate measurement of prey angular size. Stabilizing the prey image before takeoff (Figures 2D and 2E) should make prey angular size substantially easier to determine. Finally, during the final ~ 100 mm of the flight, the prey time-to-contact must be estimated so the dragonfly can initiate capture. Time-to-contact could be determined through short-range binocular disparity or

looming of the prey-image, both of which would be facilitated by foveation.

Foveation quality can be decomposed into azimuthal and elevational components. Surprisingly, the prey-image is not stabilized equally in these two dimensions. Both during the pre-takeoff period (Figure 2D) and in flight [13], the prey image jitter in azimuth is roughly half that in elevation, yielding an elliptical foveal zone. We do not yet know whether this difference is mechanical (due to higher precision control of the neck muscles that induce yaw versus pitch movements) or optical (with a fovea physically elongated in elevation on the head itself) or strategic (under deliberate control of the dragonfly). However, the elongation of the fovea in elevation is consistent with the underlying guidance strategy used to catch prey. During flight, the dragonfly aligns its body axis and flight direction to the prey's flight path, while holding the prey overhead (Figure 1A and [13]). The prey

image drift rate indicates, to a large extent, the relative speed difference between dragonfly and prey, and occurs primarily in elevation—the axis along which the fovea is longest. For prey that can be caught, the elevational drift will rapidly decrease as the dragonfly accelerates toward the prey speed. In contrast, for excessively fast prey, the elevational drift will rapidly increase as the dragonfly struggles to reach the speeds it cannot attain. Prey drift in elevation, and the fovea's elongation along this axis, may be used to determine whether a flight is likely to be unsuccessful and should therefore be terminated.

It has been established that interception guidance in the dragonfly is based on prediction and internal models [13], and it is noteworthy that similar processes underlie the selection of prey before takeoff. The determination of prey viability is based on the coupling between prey angular size and angular speed (Figure 5E). Together the range spanned by these parameters represents a prey model, and that model could, in principle, be encoded in the angular size and speed tuning of neurons within the takeoff and steering circuitry. The prediction of the prey's overhead crossing must also have a neuronal representation. Salamanders predict prey motion using a linear extrapolation of prey position [4], perhaps via retina circuit dynamics [49], and the dragonfly might employ a similar strategy to detect the moment of overhead crossing. However, in the salamander this computation is based on prey angular velocity, over a specific integration time window. In the dragonfly it remains unclear whether prey angular velocity is used or whether the overhead crossing is anticipated approximately by prey converging inward past an elevational threshold. Clarifying the computations used for prey selection and the overhead prediction, algorithmically and at the level of neural circuits, is a major question for future studies.

The natural environment is filled with near infinite diversity, and generating behaviors that can operate robustly under all conditions is challenging. Instead, a much simpler solution is to establish rules that cause behaviors to execute only under specific conditions. In this study, we have identified the criteria by which dragonflies initiate and terminate interception flights. In 300 ms, dragonflies detect prey, orient their direction-of-gaze, assess prey angular size and speed, and time the moment of takeoff to the prey crossing overhead. These heuristics are applied not merely as sensory filters and prediction of future prey position but through active orientation of the dragonfly's head toward the prey. Taken together, these actions allow the dragonfly to select a stereotyped set of takeoff conditions from a highly variable environment. These takeoff conditions in turn increase the likelihood of interception success. It is noteworthy that the time devoted to preparatory gestures and pre-flight measurements is often as long as the flight itself. The dragonfly's heuristic rules demonstrate how complex tasks can be simplified with the appropriate preparation, even when limited by time and computational resources, and highlight how the nervous system carefully regulates the time and place at which it commits to action.

EXPERIMENTAL PROCEDURES

Animal Husbandry and Flight Arena

Dragonfly nymphs (*Plathemis lydia*) were collected from local ponds and raised in aquaria with water at room temperature ($26^{\circ}\text{C} \pm 1^{\circ}\text{C}$). The nymphs were fed

black worms (*Lumbriculus variegatus*). Freshly emerged adult dragonflies were kept in buckets for 2 days before being released into the flight arena ($5.5 \times 4.3 \times 4.6$ m, Figure S1A, see [13]) with naturalistic lighting, temperature, humidity, visual texture, and abundant fruit flies (*Drosophila virilis*). The dragonflies lived and foraged freely in this room for 1–2 weeks. Each dragonfly was marked with a 4-bit color code on its abdomen; this enabled each individual to be identified and its weight recorded every morning. For experiments, we selected dragonflies of at least 4 days old, at least 300 mg, and had gained at least 20 mg the previous day.

Real Prey Presentation

Real prey were used to assess the natural motion statistics experienced by foraging dragonflies and to verify key results established with artificial prey. We recorded 142 dragonfly pre-takeoff and interception flights to fruit flies (*Drosophila virilis*) using two high-speed video cameras (Photron SA1, 1000 fps, 1/2,000 s shutter speed). This dataset was collected and first published for a study on interception guidance [13].

Artificial Prey Presentation System

We designed a robotic pulley system that drove a bead on a monofilament fishing line at controlled speed (Figure S1B). The artificial prey was made with polypropylene tubing wrapped with retroreflective tape (Figure S1B inset). The dimensions and aspect ratio matched a fruit fly's silhouette viewed from below (2×1.2 mm). In some experiments the artificial prey size was scaled proportionally to lengths 1.6–6.0 mm. The pulley motors (Portescap, Athlonix motor) could drive the artificial prey with speeds from 0.1 to 8 m/s. The system was also motorized in z-direction and could be positioned at heights of 0.1–1.2 m above the perch platform. In a typical trial, the dragonfly was automatically detected on the perch platform by cameras. These cameras then triggered artificial prey movement at a pre-assigned height and speed (Figure S1B). At completion of the trial, the system moved to the height for the next trial and awaited the trigger signal. The motion capture system used to track dragonfly kinematics was also used to track the artificial prey. The prey presentation motors were controlled via high-resolution magnetic encoders, and these encoding readings could be used to calculate prey position when camera views were unavailable.

High-Precision Motion Capture

To measure the three-dimensional head movements of the dragonfly during prey selection, we attached miniature retroreflective markers ($750 \mu\text{m}$ in diameter) to the dragonfly's head and body (Figure S1C). Two markers were placed on the head and three on the body (the latter attached to a rigid carbon fiber frame). An array of 18 motion capture cameras (Motion Analysis Co.) was customized to track these small markers at 200 Hz, with 3-D reconstruction residuals under $200 \mu\text{m}$ (see [13] for details). Dragonflies were free to perch anywhere on the perch platform, but we triggered the artificial prey system only when the experimental dragonfly perched for at least 1 min within 20 cm of the platform midline that was directly below the artificial prey track. The artificial prey parameters were selected from a library based on natural prey statistics and were presented in a pseudo-random sequence. Prey were presented at 1 min intervals given the dragonfly still satisfied the perching condition specified above.

For the perched head saccade kinematics analyses (Figures 1 and 2C), we used data from 14 dragonflies and 250 prey presentations. For the foveation analyses that examined both pre-takeoff and in-flight head control (Figures 2D–2F, 3, 4, and 6), we used data from 9 dragonflies and 165 prey presentations (39 successful flights, 65 terminated flights, and 61 no-takeoff trials). Five dragonflies in the pre-takeoff dataset were removed as they did not take flight after any prey.

Functional Fovea

The dragonfly has a high-acuity fovea on the dorsal part of the eyes, formed by an increased angular density of ommatidia [23, 31]. We defined a functional fovea on the dorsal eye of the dragonfly, analogous to this anatomical region, based on the region of the eye where the prey image was stabilized during head tracking. For each dragonfly, we defined the center of the functional fovea, called the direction-of-gaze, as the mean position of image stabilization on the eye in azimuth and elevation, in a 100 ms window, with onset 100 ms

after the pre-takeoff head saccade. The width of the functional fovea was defined as the standard deviation in prey image drift across all dragonflies ($n = 10$), in the same time window. This region was 8° in azimuth and 16° in elevation. We found the dragonfly's direction-of-gaze at rest was oriented to align with the dragonfly's body axis in azimuth and was aimed $52^\circ \pm 8^\circ$ above horizon in elevation. This closely resembles the 54° elevation of the anatomically defined dragonfly fovea measured in related species (*Erythemis simplicicollis* [23]).

Additional information may be found in the Supplemental Experimental Procedures and [13].

SUPPLEMENTAL INFORMATION

Supplemental Information includes three figures, Supplemental Experimental Procedures, and three movies and can be found with this article online at <http://dx.doi.org/10.1016/j.cub.2017.03.010>.

AUTHOR CONTRIBUTIONS

H.-T.L. and A.L. designed the study and analysis. H.-T.L. implemented the experiments, collected the data, and performed the analyses. A.L. and H.-T.L. wrote the paper.

ACKNOWLEDGMENTS

We thank members of the Leonardo lab for support and D. Parks and the Janelia vivarium for dragonfly husbandry. We are grateful to V. Jayaraman, G. Turner, K. Longden, A. Robie, B. Mowrey, and M. Mischiati for discussions and comments on the manuscript. Elliot Imler and Paul Herold collected the published *Drosophila* prey data and provided early discussions on prey motion statistics. This work was supported by the Howard Hughes Medical Institute.

Received: November 4, 2016

Revised: February 6, 2017

Accepted: March 7, 2017

Published: March 30, 2017

REFERENCES

- Oliva, D., and Tomsic, D. (2012). Visuo-motor transformations involved in the escape response to looming stimuli in the crab *Neohelice (=Chasmagnathus) granulata*. *J. Exp. Biol.* *215*, 3488–3500.
- von Reyn, C.R., Breads, P., Peek, M.Y., Zheng, G.Z., Williamson, W.R., Yee, A.L., Leonardo, A., and Card, G.M. (2014). A spike-timing mechanism for action selection. *Nat. Neurosci.* *17*, 962–970.
- Klopsch, C., Kuhlmann, H.C., and Barth, F.G. (2012). Airflow elicits a spider's jump towards airborne prey. I. Airflow around a flying blowfly. *J. R. Soc. Interface* *9*, 2591–2602.
- Borghuis, B.G., and Leonardo, A. (2015). The role of motion extrapolation in amphibian prey capture. *J. Neurosci.* *35*, 15430–15441.
- Liden, W.H., and Herberholz, J. (2008). Behavioral and neural responses of juvenile crayfish to moving shadows. *J. Exp. Biol.* *211*, 1355–1361.
- Dangles, O., Ory, N., Steinmann, T., Christides, J.P., and Casas, J. (2006). Spider's attack versus cricket's escape: velocity modes determine success. *Anim. Behav.* *72*, 603–610.
- Card, G., and Dickinson, M.H. (2008). Visually mediated motor planning in the escape response of *Drosophila*. *Curr. Biol.* *18*, 1300–1307.
- Jun, J.J., Longtin, A., and Maler, L. (2014). Enhanced sensory sampling precedes self-initiated locomotion in an electric fish. *J. Exp. Biol.* *217*, 3615–3628.
- Williams, T.M., Wolfe, L., Davis, T., Kendall, T., Richter, B., Wang, Y., Bryce, C., Elkaim, G.H., and Wilmers, C.C. (2014). Mammalian energetics. Instantaneous energetics of puma kills reveal advantage of felid sneak attacks. *Science* *346*, 81–85.
- Scantlebury, D.M., Mills, M.G., Wilson, R.P., Wilson, J.W., Mills, M.E., Durant, S.M., Bennett, N.C., Bradford, P., Marks, N.J., and Speakman, J.R. (2014). Mammalian energetics. Flexible energetics of cheetah hunting strategies provide resistance against kleptoparasitism. *Science* *346*, 79–81.
- Cresswell, W. (1996). Surprise as a winter hunting strategy in sparrowhawks *Accipiter nisus*, peregrines *Falco peregrinus* and merlins *F. columbarius*. *Ibis* *138*, 684–692.
- Gilbert, C. (1997). Visual control of cursorial prey pursuit by tiger beetles (*Cicindelidae*). *J. Comp. Physiol. A Neuroethol. Sens. Neural Behav. Physiol.* *181*, 217–230.
- Mischiati, M., Lin, H.-T., Herold, P., Imler, E., Olberg, R., and Leonardo, A. (2015). Internal models direct dragonfly interception steering. *Nature* *517*, 333–338.
- Wilson, A.M., Lowe, J.C., Roskilly, K., Hudson, P.E., Golabek, K.A., and McNutt, J.W. (2013). Locomotion dynamics of hunting in wild cheetahs. *Nature* *498*, 185–189.
- Nishikawa, K.C. (1999). Neuromuscular control of prey capture in frogs. *Philos. Trans. R. Soc. Lond. B Biol. Sci.* *354*, 941–954.
- Catania, K.C., Hare, J.F., and Campbell, K.L. (2008). Water shrews detect movement, shape, and smell to find prey underwater. *Proc. Natl. Acad. Sci. USA* *105*, 571–576.
- Nelson, M.E., and Macciver, M.A. (1999). Prey capture in the weakly electric fish *Apteronotus albifrons*: sensory acquisition strategies and electrosensory consequences. *J. Exp. Biol.* *202*, 1195–1203.
- Temple, S., Hart, N.S., Marshall, N.J., and Collin, S.P. (2010). A spitting image: specializations in archerfish eyes for vision at the interface between air and water. *Proc. Biol. Sci.* *277*, 2607–2615.
- Hilborn, A., Pettorelli, N., Orme, C.D.L., and Durant, S.M. (2012). Stalk and chase: how hunt stages affect hunting success in Serengeti cheetah. *Anim. Behav.* *84*, 701–706.
- Kenward, R. (1978). Hawks and doves: factors affecting success and selection in goshawk attacks on woodpigeons. *J. Anim. Ecol.* *47*, 449–460.
- O'Brien, W.J., Slade, N.A., and Vinyard, G.L. (1976). Apparent size as the determinant of prey selection by bluegill sunfish (*Lepomis macrochirus*). *Ecology* *57*, 1304–1310.
- Rutz, C. (2012). Predator fitness increases with selectivity for odd prey. *Curr. Biol.* *22*, 820–824.
- Olberg, R.M., Seaman, R.C., Coats, M.I., and Henry, A.F. (2007). Eye movements and target fixation during dragonfly prey-interception flights. *J. Comp. Physiol. A Neuroethol. Sens. Neural Behav. Physiol.* *193*, 685–693.
- Miller, P.L. (1995). Visually controlled head movements in perched anisopteran dragonflies. *Odonatologica* *24*, 301–310.
- Sauseng, M., Pabst, M.A., and Kral, K.A.R.L. (2003). The dragonfly *Libellula quadrimaculata* (Odonata: Libellulidae) makes optimal use of the dorsal fovea of the compound eyes during perching. *Eur. J. Entomol.* *100*, 475–480.
- Olberg, R.M., Worthington, A.H., Fox, J.L., Bessette, C.E., and Loosemore, M.P. (2005). Prey size selection and distance estimation in foraging adult dragonflies. *J. Comp. Physiol. A Neuroethol. Sens. Neural Behav. Physiol.* *191*, 791–797.
- Sparks, D.L. (2002). The brainstem control of saccadic eye movements. *Nat. Rev. Neurosci.* *3*, 952–964.
- Olberg, R.M., Worthington, A.H., and Venator, K.R. (2000). Prey pursuit and interception in dragonflies. *J. Comp. Physiol. A Neuroethol. Sens. Neural Behav. Physiol.* *186*, 155–162.
- Kral, K. (1998). Side-to-side head movements to obtain motion depth cues: A short review of research on the praying mantis. *Behav. Processes* *43*, 71–77.
- Sobel, E.C. (1990). The locust's use of motion parallax to measure distance. *J. Comp. Physiol. A Neuroethol. Sens. Neural Behav. Physiol.* *167*, 579–588.
- Labhart, T., and Nilsson, D.-E. (1995). The dorsal eye of the dragonfly *Sympetrum*: specializations for prey detection against the blue sky.

- J. Comp. Physiol. A Neuroethol. Sens. Neural Behav. Physiol. 176, 437–453.
32. Rossel, S. (1980). Foveal fixation and tracking in the praying mantis. *J. Comp. Physiol.* 139, 307–331.
 33. Harris, C.M. (1995). Does saccadic undershoot minimize saccadic flight-time? A Monte-Carlo study. *Vision Res.* 35, 691–701.
 34. Cazettes, F., Fischer, B.J., and Peña, J.L. (2016). Cue reliability represented in the shape of tuning curves in the owl's sound localization system. *J. Neurosci.* 36, 2101–2110.
 35. Gonzalez-Bellido, P.T., Peng, H., Yang, J., Georgopoulos, A.P., and Olberg, R.M. (2013). Eight pairs of descending visual neurons in the dragonfly give wing motor centers accurate population vector of prey direction. *Proc. Natl. Acad. Sci. USA* 110, 696–701.
 36. Horridge, G. (1986). A theory of insect vision: velocity parallax. *Proc. R. Soc. Lond. B Biol. Sci.* 229, 13–27.
 37. Rossel, S. (1983). Binocular stereopsis in an insect. *Nature* 302, 821–822.
 38. Brunton, B.W., Botvinick, M.M., and Brody, C.D. (2013). Rats and humans can optimally accumulate evidence for decision-making. *Science* 340, 95–98.
 39. Land, M.F. (1997). Visual acuity in insects. *Annu. Rev. Entomol.* 42, 147–177.
 40. O'Carroll, D.C., and Wiederman, S.D. (2014). Contrast sensitivity and the detection of moving patterns and features. *Philos. Trans. R. Soc. Lond. B Biol. Sci.* 369, 20130043.
 41. Nakayama, K. (1985). Biological image motion processing: a review. *Vision Res.* 25, 625–660.
 42. Snyder, A.W., Bossomaier, T.R., and Hughes, A. (1986). Optical image quality and the cone mosaic. *Science* 231, 499–501.
 43. Wardill, T.J., Knowles, K., Barlow, L., Tapia, G., Nordström, K., Olberg, R.M., and Gonzalez-Bellido, P.T. (2015). The killer fly hunger games: target size and speed predict decision to pursuit. *Brain Behav. Evol.* 86, 28–37.
 44. Boeddeker, N., Kern, R., and Egelhaaf, M. (2003). Chasing a dummy target: smooth pursuit and velocity control in male blowflies. *Proc. Biol. Sci.* 270, 393–399.
 45. Kral, K., and Poteser, M. (1997). Motion parallax as a source of distance information in locusts and mantids. *J. Insect Behav.* 10, 145–163.
 46. Horridge, G. (1977). Insects which turn and look. *Endeavour* 1, 7–17.
 47. Maldonado, H., and Barros-Pita, J. (1970). A fovea in the praying mantis eye. *Z. Vgl. Physiol.* 67, 58–78.
 48. Hateren, J.H., and Schilstra, C. (1999). Blowfly flight and optic flow. II. Head movements during flight. *J. Exp. Biol.* 202, 1491–1500.
 49. Leonardo, A., and Meister, M. (2013). Nonlinear dynamics support a linear population code in a retinal target-tracking circuit. *J. Neurosci.* 33, 16971–16982.